



*Experiments Division*

*ALBA Project Document No:*

**EXD-BL24-GD-0001**

*EDMS Document No.*

*Created: 28/04/2006*

*Pages: 29*

*Modified:*

*Rev. No.: 1*

*Conceptual Design Report*

*of the*

*CIRCE beamline*

*at the*

*ALBA Synchrotron Radiation Facility*

*Prepared by:*

**Josep Nicolas**  
**Salvador Ferrer**  
**Eric Pellegrin**

*Checked by:*

*Approved by:*

*Distribution List*

# *Contents*

<b>OVERVIEW.....</b>	<b>4</b>
<b>1 SOURCE .....</b>	<b>4</b>
1.1 Source parameters.....	5
1.2 Flux .....	6
1.3 Source size and divergence .....	6
1.4 Source power and Front-end acceptance.....	8
<b>2 FUNCTIONAL DESCRIPTION OF THE BEAMLINE .....</b>	<b>9</b>
2.1 Beamline layout and operation mode .....	10
2.2 General description of the monochromator .....	11
2.3 PEEM branch refocusing optics.....	12
2.4 PES branch refocusing optics.....	13
<b>3 MONOCHROMATOR DESIGN .....</b>	<b>14</b>
3.1 Monochromator working domain.....	15
3.2 Grating optimization .....	15
3.3 Monochromator geometry .....	19
3.4 Geometrical acceptance .....	20
<b>4 POWER LOAD ON OPTICAL ELEMENTS.....</b>	<b>21</b>
4.1 Power load on M1 .....	21
4.2 Power load on M2.....	24
4.3 Power load on the gratings .....	25
4.4 Power density on monochromator optics at normal operation .....	26
4.5 Power downstream the grating.....	26
4.6 Cooling considerations .....	27
<b>5 DIAGNOSTICS SYSTEM .....</b>	<b>27</b>
5.1 Multilayer screen.....	27
5.2 X-ray beam position monitor.....	28
5.3 Beam diagnostic setup.....	28

---

5.4	Beam monitor .....	28
5.5	Gas cell.....	28
5.6	I <sub>0</sub> Monitor chamber .....	29
5.7	Beam diagnostics included in Exit slit setup .....	29

## Overview

CELLS is a consortium created to construct and exploit the ALBA synchrotron facility to generate X rays for basic and applied research. The facility, which will be located near Barcelona, will include a 3-GeV, low-emittance storage ring able to run in top-up mode, which will feed an intense photon beam to a number of beamlines. These are placed tangentially to the storage ring and hold the experimental facilities. One of the beamlines, CIRCE, to be implemented in the first phase of the project will be devoted to photoemission spectroscopy techniques and will have two end stations installed in two independent beamline branches: one for PEEM (photoemission microscopy) and the other for photoemission near ambient pressures. Both of them will use soft X-rays generated by a helical undulator with tunable polarization and will share the monochromator. A deflecting mirror will direct the beam to one branch or to the other.

This document is organized as follows. Chapter 1 describes the source of the beamline. In Chapter 2 the functional description of the beamline is given. The details on the design of the monochromator are given in Chapter 3. Chapter 4 is devoted to the power load on the optical elements. And finally Chapter 5 describes briefly the diagnostic system of the beamline.

## 1 Source

The source for the Circe beamline is a PPM (Pure Permanent Magnet) APPLE II helical undulator, inserted in the center of the 9<sup>th</sup> medium straight section of the ALBA storage ring. This device is capable of delivering linearly polarized light, in all the directions, as well as circularly polarized light (left-handed or right-handed).

The magnetic design of the undulator optimizes the first harmonic flux at 1100eV, in circular polarization mode, while keeping the condition of reaching 99eV or less at minimum gap for horizontal polarization. Some other constraints have been taken into account:

- The minimum magnetic gap for the ID is limited to 15.5 mm, to avoid the effect of magnetic heterogeneities, which may become uncontrollable at narrower gaps.
- The magnetic forces of the undulator, which depend on the total length and on the magnetic block size, are limited to 20kN.

The block size and the undulator length have been optimized simultaneously by means of a Simplex-based algorithm that explores the full parameter space.

As a result of the optimization the selected period for the undulator is 61.8 mm. The undulator has 27 periods, what means that the ID length is 1497mm.

The specified motor speed for the phase change mechanism is 1mm/s, so the device is able to change between left and right circular polarization in about 31s.

## 1.1 Source parameters

A summary of the parameters that define the source are given in Table 1.  $K_X$  and  $K_Y$  are the standard deflection parameters of the undulator, which are proportional to the undulator period and the magnetic field in the horizontal and vertical direction respectively. The maximum values of  $K_X$  and  $K_Y$  (for minimum gap) are detailed for the three main polarization modes (linear horizontal, linear vertical, and circular (left or right)). The minimum photon energy that can be reached, which is also detailed, as well as the spectral flux, corresponding to these given energies (calculated for a SR beam current of 250mA)

**Table 1. Parameters for the beamline source**

<b>Parameter</b>	<b>Value</b>		
Type of ID	PPM Apple II		
Period (mm)	61.8		
Number of periods	27		
Magnetic gap (mm)	15.5-90.0		
Magnetic length (mm)	1496.93		
Linear phase range (mm)	-31 to +31		
Polarization modes	C.. Left, C. Right, Linear 0°-90°		
<b>Polarization</b>	<b>Horiz.</b>	<b>Vert.</b>	<b>Circular</b>
$B_X$ (T)	0	0.64	0.51
$B_Y$ (T)	0.88	0	0.51
$K_X$	0	3.67	2.98
$K_Y$	5.12	0	2.98
Min. Energy (eV)	98	179	140
Max. Flux (Ph/s/0.1%BW@250mA)	$9.3 \cdot 10^{14}$	$9.2 \cdot 10^{14}$	$1.7 \cdot 10^{15}$

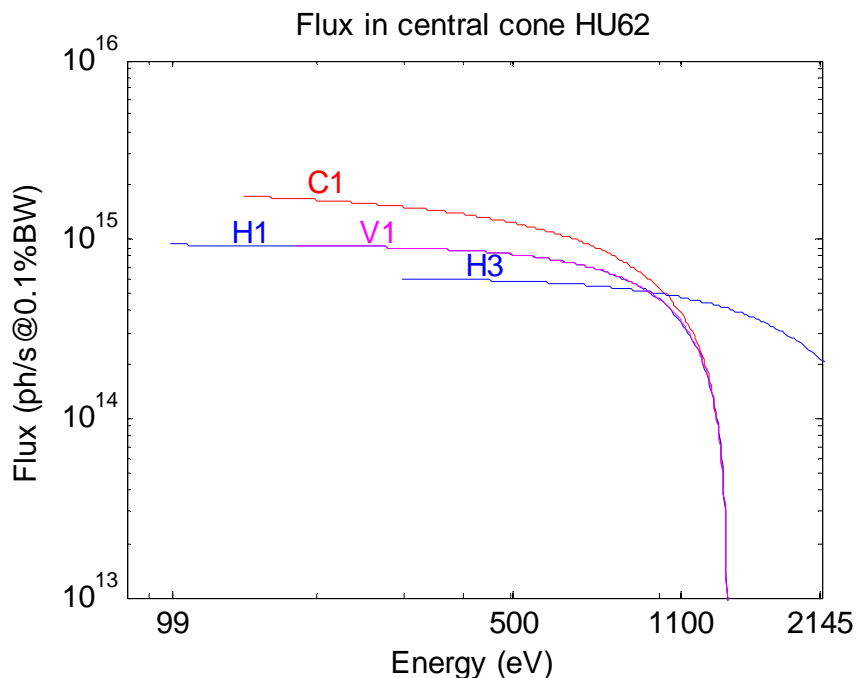


**Figure 1. Flux emitted in central cone at tuned energy. Horizontal in 1<sup>st</sup> and 3<sup>rd</sup> order and circular in 1<sup>st</sup> order are represented.**

## 1.2 Flux

The storage ring is planned to be operated at a nominal current of 250 mA, although in the future it is foreseen to operate at a maximum of 400 mA. The flux calculations given in this document are based on the nominal current (250 mA) except those regarding power, which consider the maximum achievable current, for safety reasons.

The tuning curves for the flux delivered by the HU62 (flux at tuned energy as a function of the energy) are shown in Figure 1, for horizontal polarization, in 1<sup>st</sup> and 3<sup>rd</sup> harmonic, and for circular polarization in 1<sup>st</sup> harmonic. The magnetic gap for the H1 curve varies from 15.5mm (98eV) to 50mm (1000eV). For H3 the gap at 2000eV is 40.5 mm.

The power delivered to the beamline may also impose the necessity of limiting the acceptance of the beamline to less than the central cone. This may reduce the flux at the central cone at the low energy end. This is further analyzed in Section 4.

## 1.3 Source size and divergence

ALBA is a low emittance storage ring; the beam divergence and cross section values at the center of a medium straight section are given in Table 2. As a consequence a small source and divergence can be obtained.

Table 2. Beam size at the center of ALBA medium straight sections

Quantity	RMS	FWHM
eBeam X size ( $\mu\text{m}$ )	132	310
eBeam Y size ( $\mu\text{m}$ )	7.7	18.1
eBeam X divergence ( $\mu\text{rad}$ )	48.5	114
eBeam Y divergence ( $\mu\text{rad}$ )	5.9	13.9

The FWHM spot size and divergence of the emitted photon beam are plotted in Figure 2. The red lines and the blue lines represent the vertical and horizontal dimensions, respectively. Solid lines represent the photon beam sizes and divergences, while dashed lines represent the lower limits, imposed by the electron beam. Regarding the source size, one can see that in the horizontal dimension is constant in the whole energy range, because it is limited by the electron beam. In the vertical dimension, the source size is mainly determined by the diffraction limited size of the photon beam. Therefore, it ranges from  $50\mu\text{m}$  for low energy to  $20\mu\text{m}$  for high energy. The source divergence is also energy dependent because of the diffraction limit. In the horizontal plane, the beam is diffraction limited only at low energies, so the horizontal divergence is limited by the electron horizontal divergence above  $\sim 500$  eV. In the vertical plane, the source divergence is diffraction limited at the whole energy range, and the beam divergence ranges from  $220\mu\text{rad}$  at the low energy end to  $50\mu\text{rad}$  at the high end.

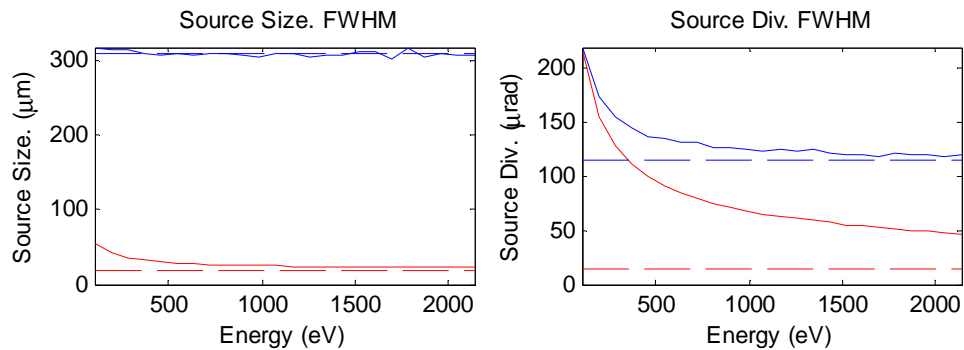
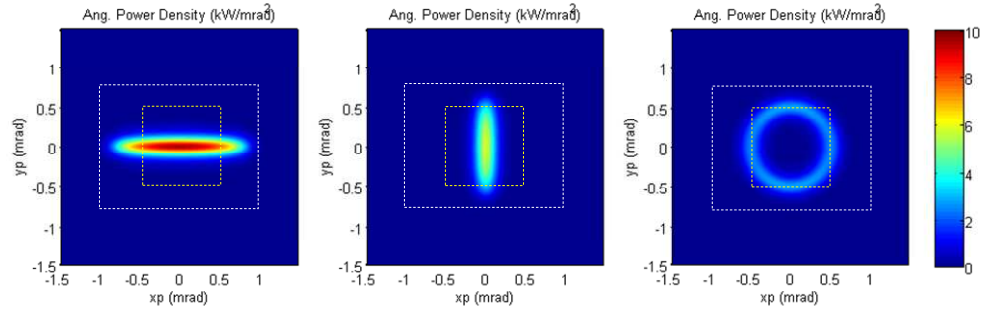


Figure 2. Spot size and beam divergence of the source. Red and blue refer to horizontal and vertical dimension respectively.

## 1.4 Source power and Front-end acceptance



**Figure 3. Angular distribution of emitted power. The white and yellow dashed frames show the acceptance of the front end first and second fixed masks, respectively.**

The power emitted by the HU62 undulator depends on the polarization mode as well as on the value of the deflection parameters (whose maxima  $K_X$  and  $K_Y$  are given in Table 1). The angular power distribution for the three main polarization modes (Horizontal, vertical and circular), at minimum gap are represented in Figure 3, this corresponds to the case when the undulator is tuned to low photon energy. One can see that the maximum power density is obtained when the undulator works in horizontal polarization configuration. A summary of the power characteristics is given in Table 3.

The frames overlapped to the power distribution given in Figure 3 represent the acceptance of the successive fixed masks of the front end. The white frame represents the first fixed mask ( $2.14 \times 1.74 \text{ mrad}^2$ ). It accepts the whole power profile, which is needed at the front-end xBPM, situated downstream. The yellow frames represent the acceptance of the second fixed mask ( $1 \times 1 \text{ mrad}^2$ ), which is the one that limits the maximum power that can be delivered to the beamline. The power delivered to the beamline can be still reduced by means of the white beam slits (movable masks) on the front end, so the values given in Table 3 are just maxima values.

When the undulator works in circular polarization mode, the power is distributed in a ring whose radius ( $\sim 0.5$  mrad for minimum gap) is determined by the  $K$  parameter, aside from a small contribution of the e-beam divergence. Nevertheless the area of interest is about  $\pm 0.15$  mrad, which correspond to the angular spread of the first harmonic. That means that for minimum gap most of the power can be removed by the white beam slits.

**Table 3. Total power emitted by HU62, for a beam current of 400 mA . Peak value of the angular power density and maximum total accepted power by the front-end (movable masks fully opened).**

Polariz. Mode	Total Power (400 mA)	Peak Power Density (400 mA)	Front End accepted power (400 mA)
	kW	kW/mrad <sup>2</sup>	kW
Horizontal	2.99	9.52	1.91
Vertical	1.54	5.80	1.25
Circular	2.03	2.81	1.22

## 2 Functional description of the beamline

The beamline will feed two experimental stations; one of them is a PEEM (Photo Emission Electron Microscope), which requires a homogeneous and intense spot on sample. The spot size should be adaptable to the field of view of the PEEM, which ranges from 3  $\mu\text{m}$  to 40  $\mu\text{m}$  (although one must consider that the incidence on the sample is at 15° glancing incidence). The other experimental station is a moderate-pressure photo-emission station (PES), which requires the maximum possible flux in a sample spot smaller than 100  $\mu\text{m}$ .

The spectral range specified for CIRCE is from 99 eV to 2000 eV, which are determined by the  $L_{2,3}$  edges of Si (99 eV) and the highest  $M_{4,5}$  and  $N_{4,5}$  edges of rare earths. The requested photon energy resolution may change depending on the experiments. Nevertheless the typical resolution that may be required is about  $E/\Delta E=6000$  (FWHM), although occasionally a resolution of  $E/\Delta E=8000$  could be requested for the PES branch.

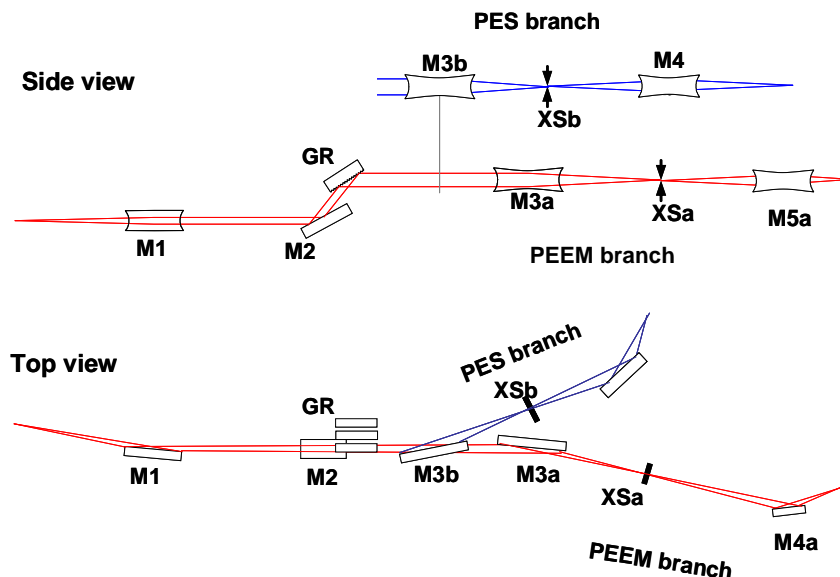


Figure 4. Sketch of the two branches for Circe beamline

The monochromator proposed for CIRCE 1s is a variable included angle plane grating monochromator (SX700-type) working with vertically collimated light. The main reasons for that election are:

- It has an extreme versatility, and for each energy it can optimize the spot size, the resolution, the flux or the harmonic rejection. It provides a wide range of possibilities and keeps the optimal condition for resolution or flux with a reduced number of gratings.
- It does not have entrance slit, what is optimal for flux optimization.
- The same grating chamber can be shared by two different exit slits by inserting different refocusing mirrors, which deflect the beam in opposite directions. This permits to split the beamline in two branches, before the exit slit. Some advantages come from this: one gains some space between the end-stations because of the early separation of the branches, no additional deflecting mirrors are needed, and no movable elements between the exit slit and the sample are needed, what contributes to keep a stable focused spot on sample.

## 2.1 Beamline layout and operation mode

The beamline is composed of two branches that share the same first mirror and the monochromator chamber. A schematic layout of the beamline is given in Figure 4. The monochromator is an entrance-slitless varied included angle plane grating monochromator, working with vertically-collimated beam. Such a monochromator is described in section 2.2. Each branch has its own exit slit, and refocusing system to gather the higher possible photon density on the sample. For the PEEM branch we have selected an ellipsoidal mirror, while for the PES branch we have considered a toroidal mirror because the required demagnification is smaller. The mirror M3b can be shifted horizontally, in and out of the beam to deflect it to the PES branch, or let it pass to the PEEM branch.

The distances, incidence angles, curvature radii (for mirrors) and footprint sizes for the different optical components, are given in Table 4. The specified labels correspond to the scheme shown in Figure 5. For M2 and GR, the changing geometry of the monochromator has been considered, so a variation range is given for the distance to previous element, and for the incidence angle, instead of a single value. In a similar way, the beam translation along M2, and the range of incidence angles have been considered to determine the footprint of M2 and on GR, but in this case only the most demanding case is given. The footprint in M3a, M3b, M4a, M5a and M4b, is also dependent on the photon energy and on the value of  $C_{ff}$ . In these cases also the most demanding case has been given, usually for low photon energy, and for high values of the  $C_{ff}$  constant.

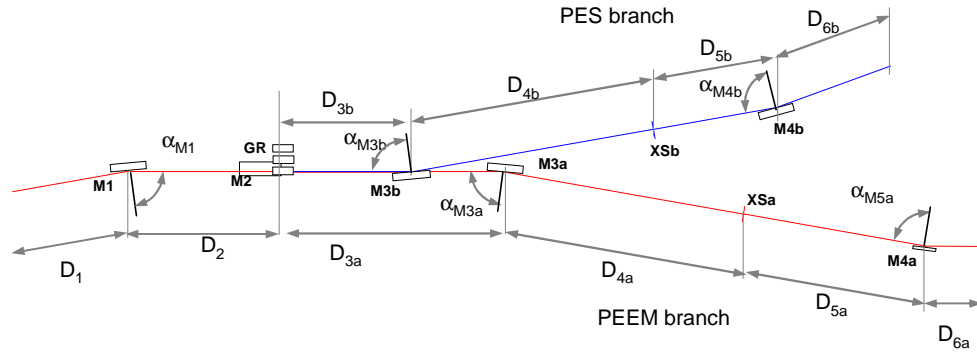


Figure 5. Scheme of the beamline with the labels corresponding to the distances and angles between the different optical elements.

## 2.2 General description of the monochromator

The main characteristic of the selected monochromator is that the grating is illuminated with vertically collimated beam, and that the included angle (the sum of the incident and exit angles) can be freely varied, without changing the position of the focal plane (the exit slit plane). In addition, because it does not need an entrance slit, it can provide high photon flux, with acceptable resolution by using few gratings in a wide energy range.

As can be seen in Figure 4, the beam, diverging from the source is horizontally deflected by a cylindrical mirror (M1). M1 is a sagittal cylinder that collimates the beam vertically. Sagittal collimation is preferred to meridional one since the thermal induced slope error has less effect in deteriorating the reflected beam. This is so since in sagittal collimation the thermal induced divergence of the reflected beam is proportional to  $2\Delta y' \cos(\alpha_{M1})$ , whereas in the meridional case it is proportional to  $2\Delta y'$ . M1 handles most of the power delivered to the beamline, and therefore must be cooled. Water cooling is the typical option, although the cooling scheme must be proposed by the bidder, on the basis of heat load and cost. After M1, the beam goes to the monochromator chamber, which contains a plane pre-mirror (M2) and a plane grating (GR), both vertically deflecting. Due to this the beam is shifted upwards in the vertical direction at the exit of the monochromator chamber. The function of the mirror M2 is to allow different incidence angles on the grating while keeping fixed the direction of the beam at the exit of the monochromator chamber. The heat load on M2 and on GR is still considerable, and although the power is much less

than in M1, the resolution of the monochromator is limited by the slope error of these elements, what means that their cooling has to be designed to minimize the effect of the heat load on the performance of the beamline. The light diffracted by the plane grating is then focused (in the two dimensions) onto the exit slit plane by a toroidal mirror (M3a for PEEM branch and M3b for PES branch), which is also horizontally deflecting.

The refocusing mirrors (M3a and M3b) corresponding to the different branches deflect the beam in opposite directions, so as to increase the angular separation between branches.

**Table 4. Summary of the positions, incidence angles and sizes of the different optical elements for Circe beamline.**

Item	Description	Distance to prev. element (mm)		Incid. angle (deg)	R (mm)	r (mm)	Footprint (mm)	
		$D_1$					Mer	Sag
M1	S.Cyl. Mirror	$D_1$	20000	88.5	$\infty$	1047	200	6
M2	Plane Mirror	$D_2$	4014-4259	82-88.8	$\infty$	$\infty$	360	8
GR	Plane Grating	$D_{2b}$	44-287	81-89.5	$\infty$	$\infty$	160	8
M3a	Torus Mirror	$D_{3a}$	4500	88.5	297355	235.6	300	26
XSa	Exit slit	$D_{4a}$	4500	--	--	--	--	--
M4a	Ellipsoidal Mir	$D_{5a}$	5000	88.5	--	--	400	15
PEEM	Sample	$D_{6a}$	1500	--	--	--	--	--
M3b	Torus Mirror	$D_{3b}$	1500	88.5	320004	261.8	300	26
XSb	Exit Slit	$D_{4b}$	5000	--	--	--	--	--
M4b	Torus Mirror	$D_{5b}$	3000	88.5	91684	62.8	190	15
PES	Sample	$D_{6b}$	2000	--	--	--	--	--

### 2.3 PEEM branch refocusing optics

The focusing requirement for the PEEM is to get a homogeneous illumination of the sample on the field of view of the PEEM, with maximum flux density. The field of view of the PEEM ranges from  $3\mu\text{m}$  to  $40\mu\text{m}$ . In addition the incidence of the x-ray beam on the sample is at about  $15^\circ$  grazing incidence, what means that the vertical dimension projection of the beam on the sample is about 4 times larger than the vertical spot size. So the spot size (RMS) should approximate as much as possible a working range between  $4 \times 1\mu\text{m}^2$  to  $40 \times 10\mu\text{m}^2$ .

An important limitation to get this spot size is the minimal distance between the last mirror pole and the sample, which is 1500 mm. That means that any mirror, with meridional slope error about  $1\mu\text{rad}$  RMS will lead to a lower limit for the spot size of  $3\mu\text{m}$  RMS, at the meridional direction of the mirror. This is the case represented in Figure 6(a), which shows the spot on sample for the PEEM, obtained by a Kirkpatrick-Baez setup in 4/1.9 vertical demagnification, and assuming meridional slope errors of  $1\mu\text{rad}$  RMS. The resulting spot size is  $36 \times 7.3\mu\text{m}^2$  (FWHM). Because of this limitation we have considered a different solution; to use a single ellipsoidal mirror, horizontally deflecting. This is shown in Figure 6(a). The mirror is setup with demagnification 5/1.5. Assuming slope errors of  $1.3 \times 10.1\mu\text{rad}^2$  (Mer $\times$ Sag) the resulting spot size is  $28 \times 3.3\mu\text{m}^2$ , which fits very well with the experiment requirements.

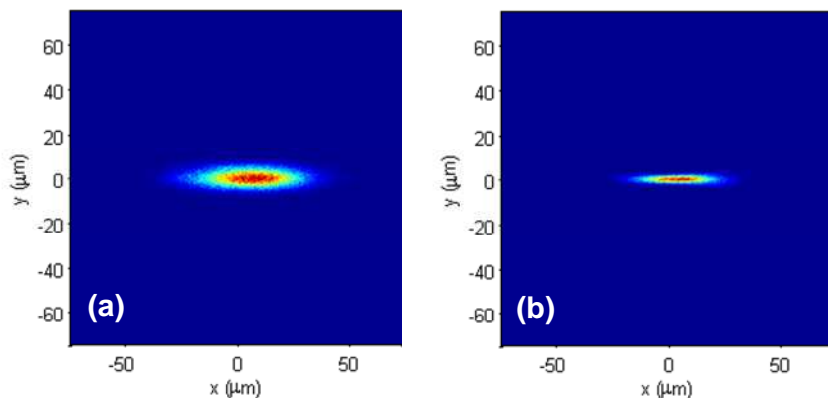


**Figure 6.** spot size on PEEM sample, for a 10 $\mu\text{m}$  slit, at  $E=793\text{eV}$ ,  $C_{ff} = 3.5$ , obtained by means of a KB mirror system (a). and a horizontally deflecting ellipsoid (b).

One additional requirement is to be able to increase the spot size on sample. This can be done by defocusing the sample. However, defocusing tends to degrade the homogeneity of the spot since the low frequency imperfections of the optical surfaces become visible as stripes. Therefore, careful attention must be paid to the low frequency part of the PSD of the mirror slope profile.

#### 2.4 PES branch refocusing optics

For the PES branch, a fixed focusing optics is considered. Nevertheless, the spot size is still variable by changing the slit size, and still depends on the  $C_{ff}$  factor and the considered photon energy. The proposed optical system is a horizontally deflecting toroidal mirror, with demagnification 1.50:1.

Considering a distance from the mirror to the sample of 2000 mm, the horizontal spot size is about 65  $\mu\text{m}$  FWHM, and because it is limited by the slope errors of the mirrors along the beamline it does not depend on the photon energy or the  $C_{ff}$  values.

The vertical spot size is quite smaller, and it depends on several factors; the working photon energy, the  $C_{ff}$  value, and the slit size. At the high energy end it can be as small as 5.7 $\mu\text{m}$  FWHM (for a 5 $\mu\text{m}$  slit), while at the low energy range it can be around 18  $\mu\text{m}$  FWHM (for a 20  $\mu\text{m}$  slit). Several cases of the resulting spot size in the PES sample are illustrated in Figure 7. At large exit slit size (S) the vertical spot size is given by the geometrical demagnification of the slit. At small exit slit size, the spot size is limited by the slope error of the mirror and by the astigmatic coma of the toroidal mirror; the coma aberration becomes important at low energies and high values of  $C_{ff}$ .

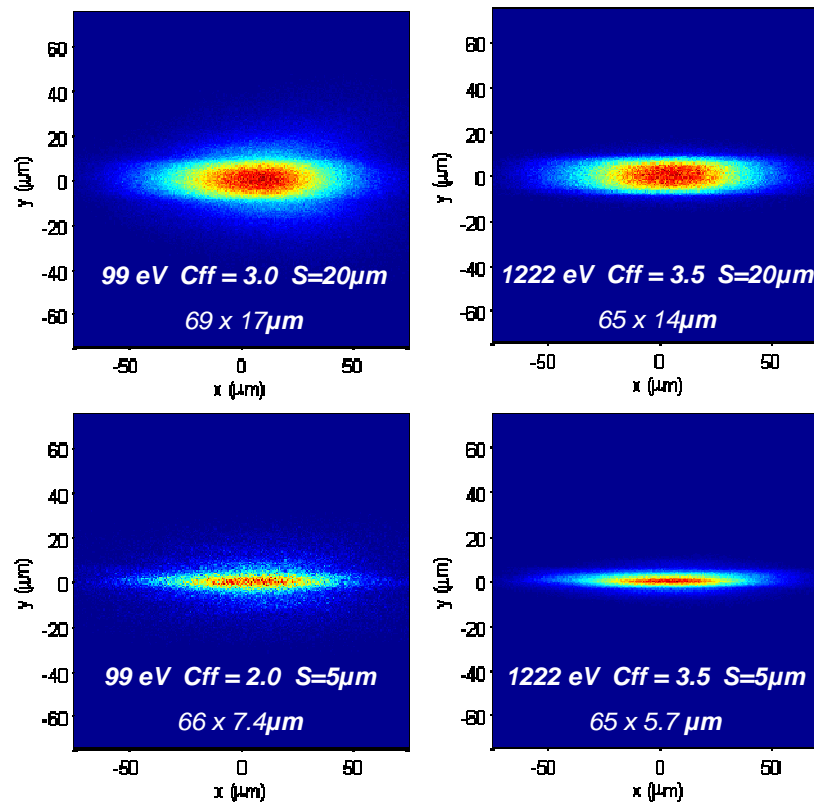


Figure 7. Spot size on sample for the PES branch, for different cases.

### 3 Monochromator design

The monochromator design involves several topics.

- Determine the distances between the different optical elements, to provide the optimal conditions for the flux-resolution tradeoff. The resulting geometry is given in section 2.1
- Determine the groove profile that optimizes the tradeoff between flux throughput and spectral resolution in the required working domain. At the same time, one establishes the working points (the value of  $C_{ff}$ ) of the monochromator that give the optimal configuration, for flux, for resolution for harmonic rejection or for any other criterion.
- Once the required working domain is defined, one determines the angular range required for the mirror M2 and the grating. This permits to design a geometry that covers the required angular range, with minimal beam deviation at the exit of the monochromator, and with maximum geometrical acceptance.

These issues are addressed in the following paragraphs.

### 3.1 Monochromator working domain

The monochromator must cover continuously the range of energies between 99eV and 2000eV. It uses three different gratings, for the low, medium and high energies respectively:

- Low Energy Grating (700 l/mm)                      99eV to 600eV
- Medium Energy Grating (900 l/mm)                500eV to 1500eV
- High Energy Grating (1200 l/mm)                900eV to 2000eV

Because the included angle is a free parameter in this monochromator, for each energy, one can change the incidence angle on the grating so as to obtain different resolution, or to optimize efficiency, or harmonic rejection, or to have different spot sizes. Therefore, the working point of the monochromator, is determined not only by the selected energy, which is given through the wavelength by the expression ( $d_0$  is the period of the grating)

$$\frac{m\lambda}{d_0} = \sin \alpha + \sin \beta, \quad (1)$$

but also by another parameter, typically the fix focus constant  $C_{ff}$ , defined as

$$C_{ff} = \frac{\cos \beta}{\cos \alpha}. \quad (2)$$

In the previous expressions  $\alpha$  and  $\beta$  are the input and output angle on the grating, measured to the grating normal, and considered to have the same sign if both incoming and outgoing rays are on the same side of the normal.

In summary, each wavelength may be monochromatized by selecting a pair of  $\alpha$  and  $C_{ff}$  values from the manifold satisfying (1) and (2). The selection is done on the basis of optimizing either energy resolution, transmission of the monochromator or harmonic rejection for a given exit slit size. This is the nice flexibility of this monochromator design not available in other schemes. In what follows we will show that the suitable values of  $C_{ff}$  that optimize efficiency, resolution and harmonic rejection take values in a reduced domain:

- Values of  $C_{ff}$  between 1.1 and 5 for positive diffraction orders.
- Values of  $C_{ff}$  between 0.2 and 0.9 for negative diffraction orders.
- $C_{ff}=1$  for specular reflection, used only for alignment purposes.

### 3.2 Grating optimization

The grating profile has been optimized at the same time as the distance ( $D_4$ ) between the refocusing mirror (M3a, M3b), and the exit slit. The selection criterion is to provide the maximum possible flux throughput, at a fixed resolution of  $E/\Delta E=8000$  (the highest needed), and a fixed slit size of  $S=5\mu\text{m}$  (the smallest). For the optimization we have used the *relative flux throughput* as the cost function. It is *defined* as the ratio of the photon flux transmitted by the monochromator, to the incoming photon flux, and integrated over the same narrow bandwidth. The goal of the optimization is to determine among the possible combinations of groove-density, groove depth and  $D_4$ -distance that provide the same resolution, those that deliver the maximum relative flux throughput. In the optimization process, an analytic model has been considered to determine the resolution for each monochromator configuration, while the

diffraction efficiency has been calculated by the differential method by Nevière.

**Table 5. Slope errors assumed in the monochromator optimization.**

Optical element	Slope Error ( $\mu\text{rad RMS}$ )	
	Meridional	Sagittal
M1	4.5	15
M2	0.75	2.5
GR(1,2,3)	0.75	2.5
M3	1.5	5

For the given layout, and assuming the slope errors for the optical elements given in Table 5 the resolution of the monochromator is limited by the slope error of the grating, or the monochromator pre-mirror (M2), at most energies and  $C_{ff}$  values. (and for the astigmatic coma introduced by M3 at low energy)

An illustration of the optimization is given in Figure 8. The flux throughput as a function of the distance  $D_4$ , is given for three significant energies. For a fixed resolution of  $E/\Delta E=8000$ . The corresponding groove density is indicated as labels at the points in the curve.

One can see that the flux throughput reaches its peak value at distances between 4 and 6 meters, for the three considered energies. Shorter values of  $D_4$  have limited flux throughput because very dense gratings are needed to disperse the wavelength enough to be resolved, and dense gratings have limited diffraction efficiency. In the other end, at very long distances the flux throughput decreases also. This is because although sparser gratings are efficient, the monochromatic spot size increases due to the slope errors.

Since the distance has to be fixed for the whole energy range, we have considered the following values

- PEEM Branch  $D_4 = 4.5\text{m}$
- PES Branch  $D_4 = 5.0\text{m}$

The slight difference between them is due to the slightly higher resolution demands of the PES station.

**Table 6. Grating profile parameters for the three selected gratings**

	Groove Density (l/mm)	Groove Depth (nm)	Groove to period ratio (%)
Low	700	15	75
Mid	900	9	75
High	1200	7	75

The grating groove density, groove depth, and groove to period ration of the selected solutions are detailed in Table 6 . They correspond to the solutions that

come from the optimization (the groove density of the high energy grating has been slightly increased so as to reach good resolution at higher energies).

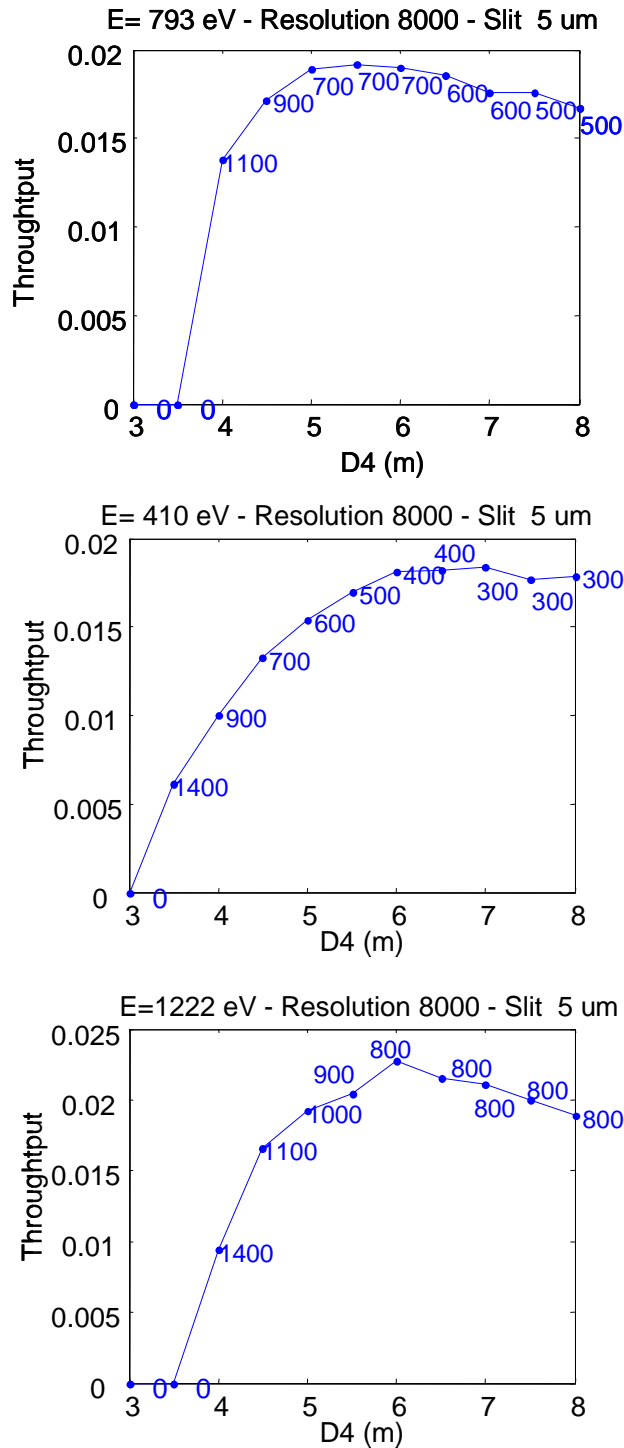


**Figure 8. Flux throughput after the monochromator as a function of the D4 distance, for fixed resolution, and fixed Cff. Energies representative of the three ranges are considered.**

These three solutions provide good diffraction efficiency in the required energy ranges (diffraction efficiency defined as the ratio of the intensity diffracted to

the 1<sup>st</sup> order to the incoming intensity, for a monochromatic wave). This is shown in Figure 9, where the diffraction efficiencies for the gratings are plotted for a value of  $C_{ff}=2$ .

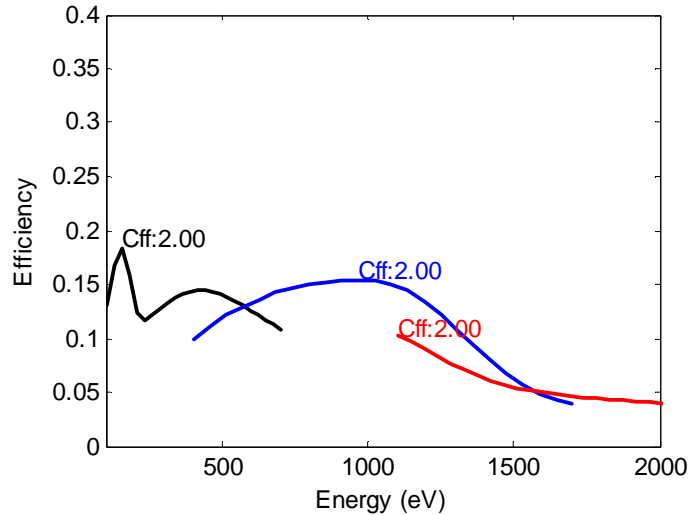


**Figure 9. Grating diffraction efficiency for the three selected gratings.**

The resolution, which depends on the spot size at the exit slit plane and on the vertical aperture of the exit slit is plotted in Figure 10. One can see that slit sizes between 5  $\mu\text{m}$  and 30  $\mu\text{m}$  are to be used to reach spectral resolutions between 3000 and 8000 ( $E/\Delta E$  FWHM)

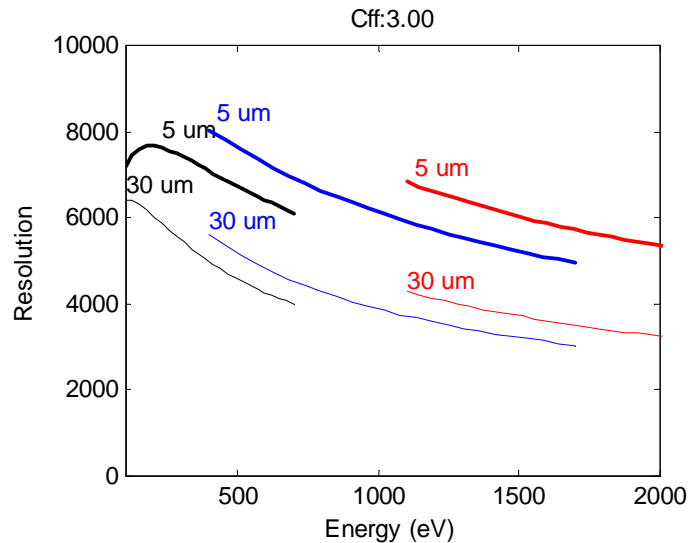


**Figure 10. Resolution provided by monochromator at fixed exit slit size**

The flux through the exit slit depends not only on the grating diffraction efficiency, but also on the reflectivity of the monochromator pre-mirror, and on the size of the exit slit. Because of this, it is useful to consider also the relative throughput, since it quantifies not only the diffraction efficiency and the reflectivity of the mirrors but also the acceptance of the exit slit.

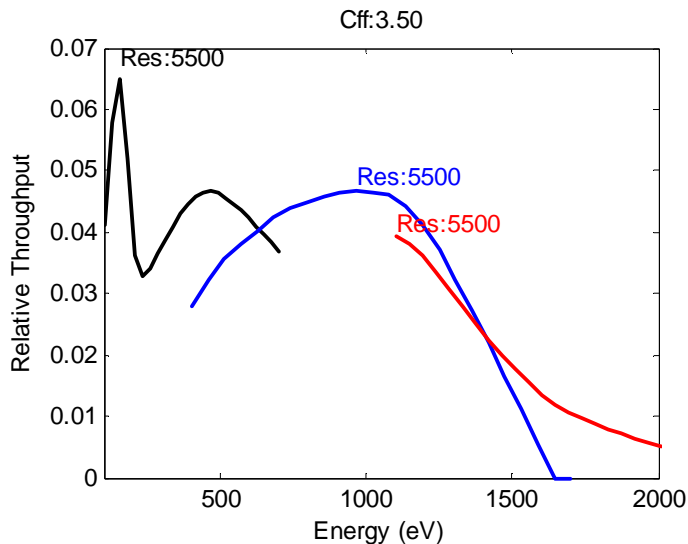


**Figure 11. Relative throughput for the different spectral resolutions at two resolutions.**

The relative throughput for the monochromator considered is represented in Figure 11, for a  $C_{ff}$  value of 3.5, over the whole required energy range, and for a moderate resolution. To reach higher resolution, the slit size has to be smaller, and the relative throughput is reduced,

### 3.3 Monochromator geometry

The angular range allowed for the monochromator pre-mirror M2 and for the grating (GR) determines the working domain of the monochromator. These angular ranges are given in Table 4. To increase them is useless since the acceptance of mirror M2 and of the grating GR is zero outside these limits. This is a consideration that has to be taken into account to determine the geometry of the monochromator; another consideration is to minimize the excursions of the beam after the monochromator.

The energy scan is performed by the rotation of the pre-mirror M2 and of the grating GR. The rotation axis for the grating is located at the center of its surface, as illustrated in Figure 12. The rotation axis RM2 of the mirror is selected to minimize the vertical excursion of the beam, on the whole angular range of the mirror. The results for such an optimization for the selected angular range are given in Table 7.

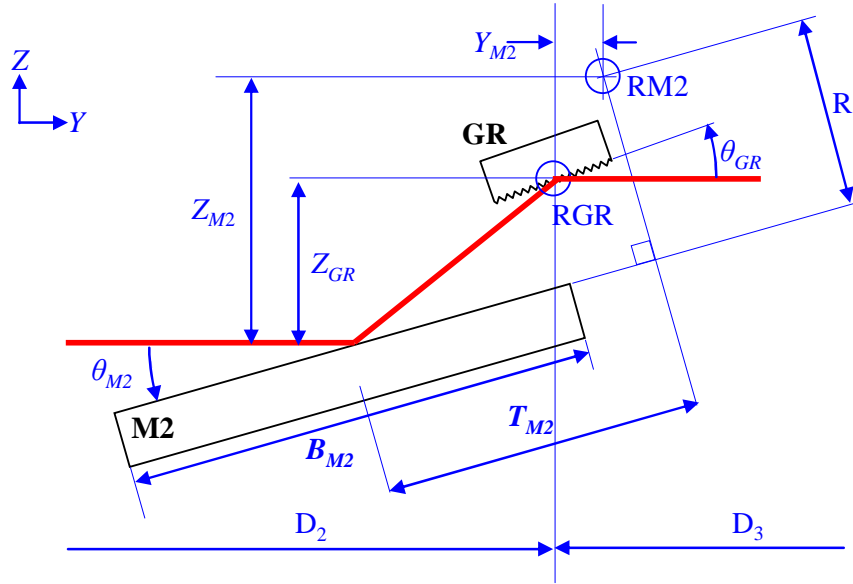


Figure 12. Scheme of the monochromator layout.

The position and length of the pre-mirror are optimized to fit the  $(E, C_{ff})$ -region of geometrical acceptance of the beamline with the optimal working region for each grating.

Table 7. Geometric parameters of the beamline.

Parameter	Value	Unit
$Z_{GR}$	15.00	mm
$Z_{M2}$	22.55	mm
$Y_{M2}$	0.001	mm
$R$	15.05	mm
$T_{M2}$	208	mm
$B_{M2}$	365	mm

### 3.4 Geometrical acceptance

The geometrical acceptance of the beamline is the fraction of the beam that is accepted in the active area of the optical elements. The selected monochromator geometry, and mirror sizes determine a finite region of the  $(E, C_{ff})$  domain in which the acceptance is significant, This is represented in Figure 13. For the 700 l/mm grating, an acceptance close to 1 in the low energy range is reached for  $C_{ff}$  values between 1.5 and 5. For the 900 l/mm grating and the 1200 l/mm grating the acceptance is close to one in the medium and high energy ranges for values of  $C_{ff}$  between 1.2 and 5. One may see that the angular range defined by these limits fits with the region of acceptance of the mirror.

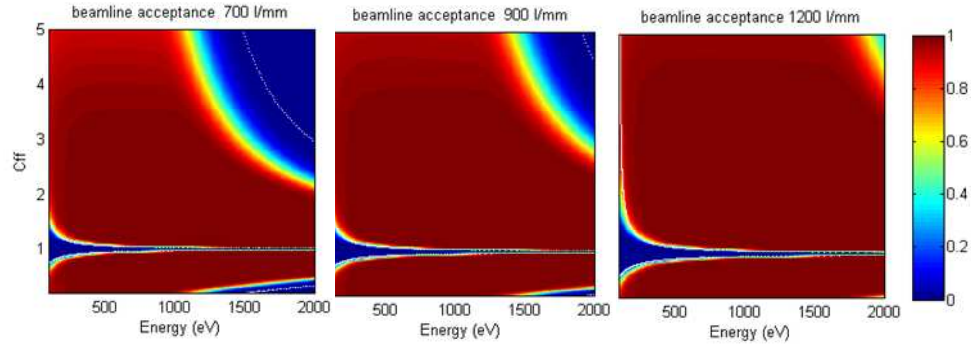


Figure 13. Geometrical acceptance of the beamline and limits established by the grating and the premirror angular range.

## 4 Power load on optical elements

### 4.1 Power load on M1

The insertion device reaches its maximum emitted power for high magnetic fields, i.e. for small gap. This is when it is tuned to low photon energies, since, in addition to the fundamental order, higher order harmonics carry on significant power. A part of the generated power is stopped by the white beam slits inside the storage ring tunnel, although when they are fully opened they may accept 1.9kW (for horizontal polarization mode). The maximum front-end acceptance is considerably larger than the source divergence at minimum energy. This means that a significant quantity of power can be removed from the beamline by reducing the acceptance of the white beam slits without loss of flux on sample. The optimal tradeoff between flux acceptance and power acceptance is shown in Figure 14, for minimum gap, in horizontal polarization mode. One can see that more than a 90% of the photon flux of the central cone is accepted in a less than  $0.25 \times 0.25 \text{ mrad}^2$  acceptance, and that the power accepted within is about 400W at 400mA. The remaining power  $\sim 1600\text{W}$  must be absorbed by the primary slits when they are delimiting the beam, or by a water cooled fixed mask upstream M1 (but downstream the 1<sup>st</sup> diagnostics set).

Nevertheless, one must take into account that on the limits of the power distribution footprint on M1 there is a steep temperature gradient and consequently a significant thermally induced slope error. Therefore, in order to avoid flux loss, one wants to keep the power footprint limits away from the flux footprint (given by the source size and divergence). That is, a larger acceptance has to be foreseen, for instance  $0.3 \times 0.3 \text{ mrad}^2$ . One can see in Figure 14 that in this case M1 must stand an incident power of about 600W.

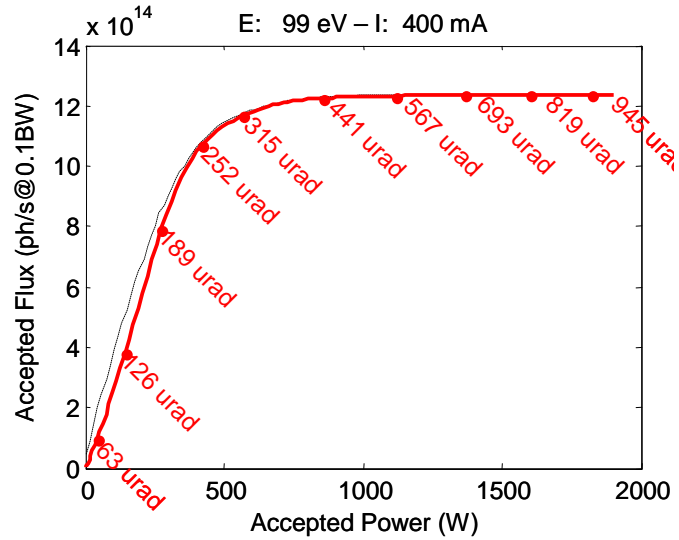


**Figure 14.** Tradeoff between Power accepted and flux accepted for minimum gap configuration at horizontal polarization mode, considering square slit. The labels indicate the slit acceptance. The dashed black line indicates the optimal tradeoff (a different horizontal to vertical ratio of the slit for every size).

The fraction of the incident power that is absorbed in M1 depends on the gap of the undulator; for small gap, tuned at low photon energy, the K values are large, what means, that high harmonics carry a lot of power: Since the cutoff energy of M1 is slightly above 2KeV, most of the power is absorbed. For larger gaps (ID tuned at higher photon energy) the K values are smaller, and the power emitted by the source decreases a lot. Nevertheless, all the power is contained in only a few harmonics, and that means that a smaller fraction of the total power is absorbed in M2. Figure 15 shows the incoming and absorbed power accepted by M1 as a function of the ID tuned energy (1<sup>st</sup> harmonic). An acceptance of  $0.3 \times 0.3 \text{ mrad}^2$  is considered in the calculation. The maximum incident power occurs at minimum gap (515 W), and most of the power is absorbed (460 W). The incident power decreases rapidly for higher photon energy (285W at  $C_K=284\text{eV}$  and 127W at  $\text{Fe}_{L3}=706\text{eV}$ ) and so does the absorbed power (221W at  $C_K$  and 70W at  $\text{Fe}_{L3}$ ).

Also the power density on the mirror surface is an important issue. The dependence of the peak power density with the photon energy tuned in the ID is given also in Figure 15. One can see that a quite significant value is reached for minimum gap - about  $0.41/0.45 \text{ W/mm}^2$  (absorbed/incident). But also in this case the value decreases a lot for larger tuned energies:  $0.20/0.25 \text{ W/mm}^2$  at  $C_K$  and  $0.08/0.12 \text{ W/mm}^2$  at  $\text{Fe}_{L3}$ .

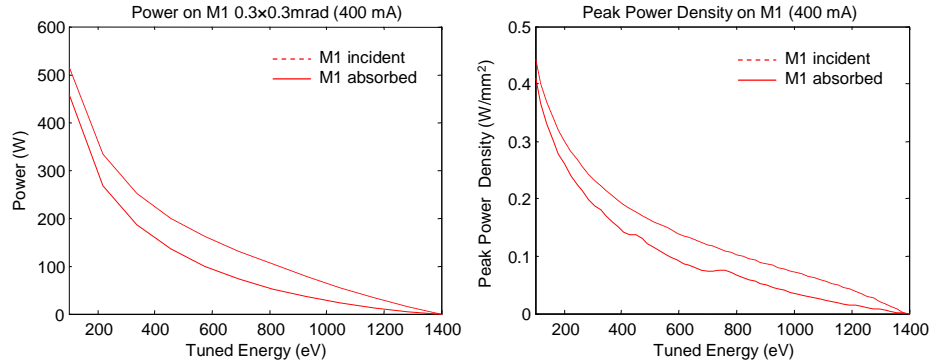


**Figure 15.** Power delivered onto the first optical element of the beamline. At the left, the total incident power and the total absorbed power is plotted as a function of the tuned energy in the source. The corresponding peak power density is given in the plot at the right.

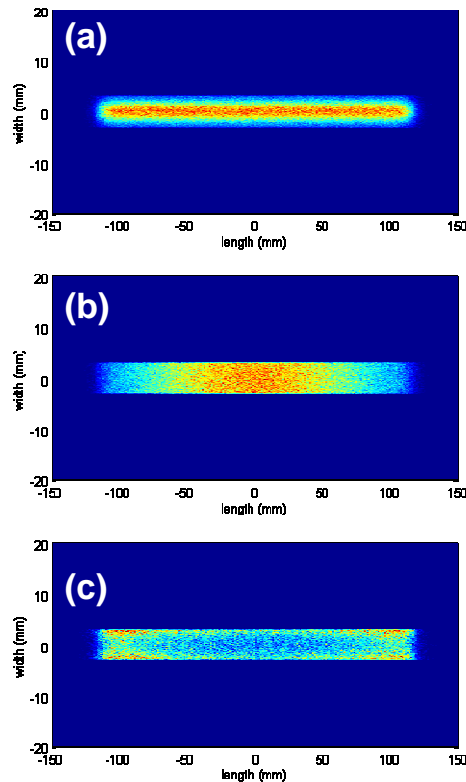


**Figure 16.** Power footprint in M1 for minimum gap, for a front end acceptance of  $0.3 \times 0.3 \text{ mrad}^2$ . (a) horizontal polarization (b) vertical polarization, (c) circular polarization.

The footprint in M1 of the power distribution is given in Figure 16 for the three main polarization cases of the ID at minimum gap. One can see that the power distribution is quite different in the three cases. For linear polarization in the horizontal plane – Figure 16 (a) – the power profile is almost constant along longitudinal direction, and normally distributed along the sagittal direction. For vertical polarization – Figure 16 (b) – the power footprint is Gaussian along the mirror and constant across it, in the region given by the primary slits.

The case of circular polarization is completely different, since the peak power density appears at the edges of the footprint limited by the primary slits.

## 4.2 Power load on M2

The power load analysis on M2 is a major design issue for this beamline for a number of reasons.

- Its meridional slope error is a limiting factor for the spectral resolution of the monochromator. Therefore one wants to minimize the figure error induced by the thermal deformation of the mirror.
- The incidence angle and the point of incidence of the beam on the mirror surface changes during the energy scans of the monochromator. So the thermal effects have to be limited to avoid drifts that come from the thermal relaxation after the heat load position has changed.

The total power that reaches M2 is less than 70W, and the amount of absorbed power depends on the incidence angle (which is very steep for low photon energy and low values of  $C_{ff}$ ). The total power absorbed by M2 is represented in Figure 17 as a function of the undulator tuned energy, for the minimum and maximum incidence angle on M2. These are the most demanding case, although they do not represent a typical configuration during normal operation. One can see that almost all the power is absorbed in M2 when it is at its minimum incidence angle (82.0°), that is about 70W. For the most grazing incidence (88.8°) the absorbed power decreases below 30W.

It is important to note that although the total power emitted by the source decreases very rapidly with the ID tuned energy, the power in M2 is sustained up to 700eV. This is because the spectral distribution of the undulator changes with the gap, and more power is emitted at the low photon energies that are reflected by M1.

The power density on M2 is also represented in Figure 17. Some oscillations appear on the plot, they come from the drop on the reflected power at M1 when the different harmonics fall in the ~2200eV absorption edge of gold. Nevertheless, these oscillations are dimmed by the emittance effects on the source, which are not considered in these calculations. One can see that the power density is a critical issue, since it can reach very significant values. The most demanding case is when the mirror is at an incidence angle of 82°. The power density reaches values about 0.25W/mm<sup>2</sup> while for 88.8°, it hardly reaches values about 20mW/mm<sup>2</sup>. This is much smaller because of two reasons: the power footprint is much larger and the reflectivity at grazing angle is larger.

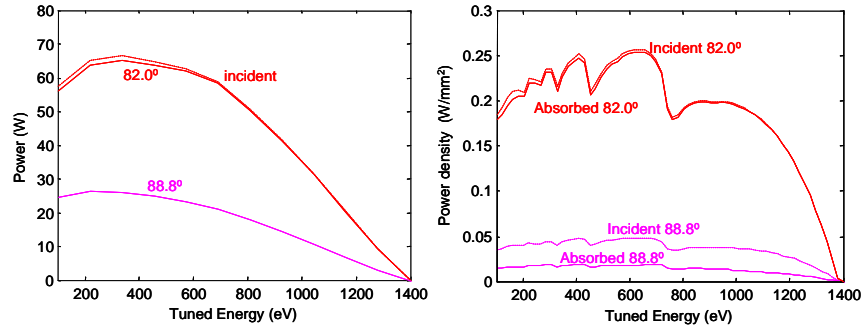


Figure 17. total power and power intensity in M2 as a function of the ID tuned energy. The two limit incidence angles for M2 are represented.

### 4.3 Power load on the gratings

The power load on the grating is also an important issue since it is also a limiting factor for the spectral resolution of the monochromator. Nevertheless, the footprint is not so changing in this case and the total amount of power is much smaller than in M2.

To calculate the power absorption of the grating we have approximated the grating to a mirror (we have calculated the reflectivity of a gold coated mirror at the input angle of the mirror). This is not a very accurate approximation but avoids a very heavy calculation.

The maximum power is delivered to the grating when M2 is at its most grazing incidence, which is when the incidence angle in M2 is 88.8°. In that case the power delivered to the grating is about 40W. These can be absorbed or diffracted (mainly reflected to the zero order) depending on the incidence angle on the grating. The two extreme cases are represented in Figure 18. When the grating is at its most grazing incidence, 89.5°, only 5W are absorbed, and the rest are diffracted to the zero order stop and the optics downstream. The opposite case occurs when the grating is at its most normal incidence, at 81.0°; in this case almost the 40W are absorbed in the grating. Although these quantities are very large, they are the extreme cases, and are far from the power and power densities usual during operation.

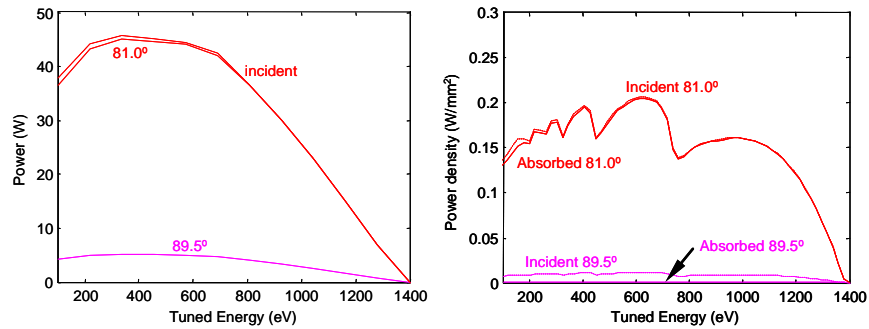


Figure 18. Power and power density on the grating for the two extreme incidence angles.

#### 4.4 Power density on monochromator optics at normal operation

The power and power density values given in the previous sections correspond to the most demanding case, when the mirror absorbs all the power, or when it transmits most of the power to the grating, and it absorbs it. Nevertheless, those angle configurations do not correspond to a practical configuration, and only indicate the maximum power load that the optics needs to handle, in case of accident. In normal operation, when the mirror pitch and the grating pitch are coordinated the power density on the optics is much smaller.

The power density absorbed by M2 and GR (700l/mm) is represented in Figure 19 as a function of the working point of the monochromator. One can see that only at very low energy, and low  $C_{ff}$  the power density absorbed in M2 is above  $0.15 \text{ W/mm}^2$ , which is significantly less than the  $0.25 \text{ W/mm}^2$  that could be absorbed in case of accident. This is also the case for the power density absorbed in the grating. In this only  $0.012 \text{ W/mm}^2$  are absorbed (in the low  $C_{ff}$  section at medium energy) what can be easily handled with a side cooling scheme.

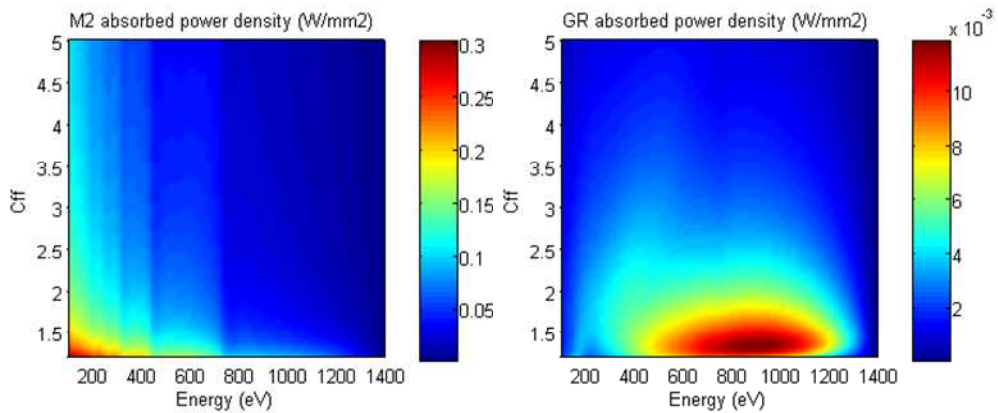
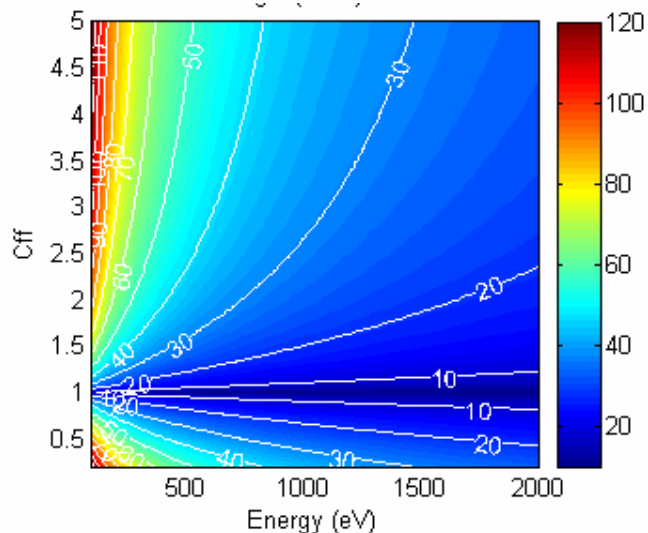


Figure 19. Power density absorbed in M2 and GR as a function of the tuned energy and the selected  $C_{ff}$  factor.

#### 4.5 Power downstream the grating

Most of the power is carried in the zero order, which must be absorbed in the zero order stop downstream the grating. Nevertheless, a part of it could propagate to the refocusing mirrors (M3b, M3a). In that case a considerable amount of power would be delivered to these mirrors, and therefore they would require some cooling.



**Figure 20. Angular deviation of the zero order from the horizontal, for a 700 l/mm grating.**

#### 4.6 Cooling considerations

The total power, and power density delivered to the beamline optical elements indicates that water cooling is needed to keep the slope errors at acceptable values. Internal channel cooling is suggested for M1, which is under higher power load. Side cooling system for M2 and the gratings should be good enough. Nevertheless, given the relatively high power density an internal cooling solution should also be considered for M2. To determine a final solution one needs to perform the finite element analysis simulation of the thermally induced slope errors.

Refocusing mirrors M3 may need cooling, in this case side cooling is suggested.

Exit slits, beam defining slits and beam position monitors, mirror masks, zero order baffle and photon shutters will be water cooled wherever is necessary.

Temperature monitors will be placed on every vessel and in the mirror blanks of water cooled mirrors.

### 5 Diagnostics system

Several types of devices for photon beam monitoring along the CIRCE beamline are to be installed, some of them are offline, that means cannot be used during data collection, and some other are online devices, that is, are to be used during data collection. A brief description of each of these components is given below.

#### 5.1 Multilayer screen

It consists on a cooled multilayer mirror deflecting the undulator radiation by 90° onto a phosphor-coated view port, where the optically visible beam footprint is recorded with a CCD camera. Therefore, even being illuminated

by the white beam, the multilayer reflects a limited band of energies, in such a way that a much narrower spot size, fully transmitted by the front end can be used for monitoring the photon beam position.

This is an offline diagnostics device.

## 5.2 X-ray beam position monitor

X-ray beam position monitor (xBPM, BESSY II or similar design; see K. Holldack et al., AIP conference proceedings 521, 354 (2001)): It consists on a Two-dimensional blade monitor with four isolated tungsten blades mounted at an angle of, e.g., 45 degree each with respect to the vertical direction inside a photon beam opening within a cooled OFHC copper block.

Blade angles and distances are optimized according to spectral and angular characteristics of undulator with respect to parasitic dipole radiation. The Readout of photocurrent is done using LCAD-4 four-channel electrometer including negative bias voltage on tungsten blades.

This is an online diagnostic system.

## 5.3 Beam diagnostic setup

The beam diagnostics setup: consists of a six-way cross with a linear feedthrough including fluorescent screen and an isolated high-transmission tungsten mesh for the white beam section, or gold mesh for the monochromatic beam section mesh. The fluorescent screen and the mesh are fully retractable from the photon beam path.

## 5.4 Beam monitor

The beam monitor consists of a six-way cross with a linear feedthrough which includes a thin film metal sample that partially intercepts the monochromatic beam. The drain current is measured in order to monitor the selected photon energy and polarization during data collection..

This is an online diagnostic system.

## 5.5 Gas cell

In order to calibrate the spectral resolution of the monochromator a gas cell will be included at each branch of the beamline.

Each gas cell consists of a 6-way cross including cylindrical gas ionization chamber, a leak valve, and a channeltron detector. Both the beam entrance and exit ports include one pair of aperture disks each, with small beam orifice for differential pumping between aperture disks. Alternatively, window gate valves with thin Al windows may be used instead of the differentially pumped orifices.

This is an offline diagnostic system.

## 5.6 $I_0$ Monitor chamber

This is a small vacuum chamber that includes a rotary feedthrough with a fluorescent screen and a high-transmission gold mesh, and a photodiode. The mesh arrangement includes a drain current setup (BNC feedthrough, UHV-compatible Kapton-insulated coaxial cable).

In addition a Gold evaporator is installed inside the vacuum chamber for deposition of fresh gold layers on the gold mesh.

## 5.7 Beam diagnostics included in Exit slit setup

The exit slit setups will also include some diagnostic consisting on two-jaw horizontal aperture (manual) upstream the exit slit blades. The aperture jaws will be electrically isolated with respect to ground and will include a drain current setup for future PID -controlled feedback loop of M3a and M3b pitch adjustments based on differential current measurement from horizontal aperture jaws).